Multislice Cardiac Arterial Spin Labeling Using Improved Myocardial Perfusion Quantification with Simultaneously Measured Blood Pool Input Function

Adrienne E. Campbell-Washburn,[1,2]* Hui Zhang,[3] Bernard M. Siow,[1,3] Anthony N. Price,[4] Mark F. Lythgoe,[1] Roger J. Ordidge,[5] and David L. Thomas[6]

Purpose: Myocardial blood flow (MBF) is an important indicator of cardiac tissue health, which can be measured using arterial spin labeling. This study aimed to develop a new method of MBF quantification with blood pool magnetization measurement ("bpMBF quantification") that allows multislice cardiac arterial spin labeling.

Theory and Methods: A multislice segmented ECG-gated Look-Locker T_1 mapping sequence was validated. Quantification of multislice arterial spin labeling is not straightforward due to the large volume of blood inverted following slice-selective inversion. For bpMBF quantification, a direct measurement of the left-ventricle blood pool magnetization was used to approximate the blood input function into the Bloch equations. Simulations and in vivo measurements in the mouse heart were performed to evaluate the bpMBF method.

Results: Measurements indicated that blood pool magnetization requires ~3 s to return to equilibrium following slice-selective inversion. Simulation and in vivo results show that bpMBF quantification is robust to variations in slice-selective thickness and therefore applicable to multislice acquisition, whereas traditional methods are likely to underestimate multislice perfusion. In vivo, single and multislice perfusion values matched well when quantified using bpMBF.

Conclusion: The first multislice cardiac arterial spin labeling technique has been presented, which can be used for accurate perfusion measurements in studies of cardiac disease. **Magn Reson Med 70:1125–1136, 2013. © 2012 Wiley Periodicals, Inc.**

Key words: arterial spin labeling; perfusion; look-locker; cardiac; multislice; perfusion model

Noninvasive preclinical imaging offers unparalleled opportunities to study cardiac structure and function in vivo, and as such has become essential in the study of experimental models of cardiovascular disease (1,2). Emphasis has been placed on developing fast, specific, and sensitive MRI methods for these studies. Perfusion, or capillary level blood flow, is an important tissue parameter, which can be measured noninvasively using arterial spin labeling (ASL) (3). Currently, ASL data can only be acquired in a single slice when applied to the heart. The ability to measure myocardial blood flow (MBF) in multiple slices would be greatly advantageous in characterizing disease models. However, quantifying perfusion in the multislice case is not straightforward.

A single slice pulsed ASL technique (flow alternating inversion recovery) comparing T_1 recovery following global and slice-selective inversion has been implemented in the mouse and rat heart, and applied in many preclinical cardiovascular studies (4–22). When moving to the multislice scenario, a wider slice-selective inversion is required to measure T_1 in all slices. This results in the inversion of a large volume of blood in the heart and lungs and therefore changes the input function of the blood magnetization into the myocardium.

In this study, we present a multislice segmented ECG-gated Look-Locker T_1 mapping sequence, which generates multislice data in the same scan time as the single slice acquisition. We develop a new method of quantifying perfusion using a measurement of the blood magnetization from the blood pool. This method will be referred to as the blood pool MBF (bpMBF) quantification method. Simulation studies (guided by in vivo data acquired in the mouse heart) are used to investigate the effects of the blood magnetization input function on MBF measurements and to investigate the sensitivity of the quantification method. Our simulation and in vivo results imply that the bpMBF quantification is robust to variations in slice-selective inversion thickness and is therefore applicable to multislice ASL perfusion mapping. We note that that perfusion is likely to be underestimated using traditional quantification methods if the model assumptions are not carefully obeyed, especially when moving to thicker slice-selective inversions for the multislice case. This study presents the first multislice perfusion measurements in the mouse heart using MRI.

THEORY

Myocardial perfusion measurements with ASL are based on the difference between T_1 recovery under two

[1]Centre for Advanced Biomedical Imaging, Division of Medicine and Institute of Child Health, University College London, UK.

[2]Department of Medical Physics and Bioengineering, University College London, UK.

[3]Centre for Medical Image Computing, Department of Computer Science, University College London, UK.

[4]Division of Imaging Sciences and Biomedical Engineering, King's College London, King's Health Partners, St. Thomas' Hospital, London, UK.

[5]Centre for Neuroscience, University of Melbourne, Melbourne, Australia.

[6]Department of Brain Repair and Rehabilitation, University College London, Institute of Neurology, Queen Square, London, UK.

Grant sponsors: British Heart Foundation, Engineering and Physical Sciences Research Council. Adrienne Campbell-Washburn is a Commonwealth Scholar funded by the Department for Business, Innovation and Skills (UK Government).

*Correspondence to: Adrienne E. Campbell-Washburn, B.Sc., UCL Centre for Advanced Biomedical Imaging, Paul O'Gorman Building, 72 Huntley St, London WC1E 6DD, UK. E-mail: adrienne.campbell.09@ucl.ac.uk

Received 1 August 2012; revised 17 September 2012; accepted 6 October 2012.

DOI 10.1002/mrm.24545

Published online 20 November 2012 in Wiley Online Library (wileyonlinelibrary.com).

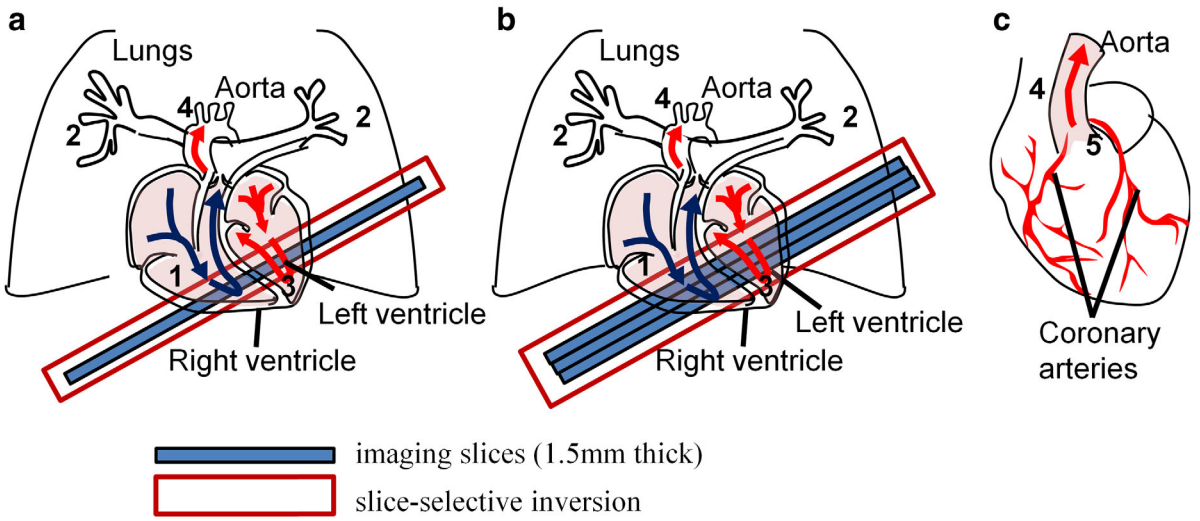

FIG. 1. Schematic diagram showing the slice-selective acquisition for the (**a**) single slice and (**b**) multislice case. A much larger volume of blood in the left ventricle, right ventricle, and lung is inverted in the multislice case. The diagrams also demonstrate the circulation through the heart and lungs: (1) deoxygenated blood circulates through right ventricle to the lungs, (2) blood in the capillary system of the lungs becomes oxygenated, (3) blood returns to heart and into the left ventricle, (4) the left ventricular blood is pumped out through the aorta (fraction of blood ejected determined by ejection fraction), and (5) the coronary arteries branch off the aorta after the aortic valve to perfuse the myocardial tissue (**c**). [Color figure can be viewed in the online issue, which is available at wileyonlinelibrary.com.]

different conditions: following a global inversion pulse (tagged condition) and following a slice-selective inversion pulse (control condition) (4). Following the slice-selective inversion, the blood perfusing into the tissue of interest is "fresh" (i.e., fully relaxed) and therefore causes an apparent acceleration of T_1 recovery. Bauer et al., (23) modeled the effect of perfusion on myocardial T_1 recovery and Belle et al., (4) extended this model to estimate perfusion under the assumption that all inflowing blood is fresh in the slice-selective case and recovering with the T_1 of blood ($T_{1\text{blood}}$) in the global inversion case. Using this model, the T_1 values derived from curve fitting are directly compared to generate an estimate of perfusion (Eq. [1]) (4):

$$\text{MBF} = \frac{\lambda}{T_{1\text{blood}}}\left(\frac{T_{1\text{global}}}{T_{1\text{slice-selective}}} - 1\right) \quad [1]$$

where λ (the blood-tissue partition coefficient of water) = 0.95 mL/g (10), myocardial T_1 measurements following global and slice-selective inversion are indicated by subscripts and $T_{1\text{blood}}$ is taken from the left-ventricle blood pool. T_1 is typically measured in the mouse heart using a Look-Locker acquisition where a segment of k-space is acquired for each heart beat after the inversion throughout T_1 recovery (9,12,22). T_1 can be quantified from the signal recovery data using a three parameter exponential fit with Look-Locker correction factor (24).

However, the assumption of Eq. [1] that all inflowing blood is fresh after the slice-selective inversion is not always valid. When applying a slice-selective inversion slab to invert the myocardial tissue, a large volume of blood contained within the right ventricle, left ventricle, capillary bed of the lung and vessels is inverted simultaneously, particularly in the multislice case (Fig. 1a,b). The inverted blood from the right ventricle and lungs is then recirculated through the left ventricle before being pumped through the coronary arteries to perfuse the myocardial tissue [transit time from right to left heart is ~0.83 s in mice (25)] (Fig. 1). In addition, the fraction of left-ventricle blood ejected in a single heart beat (the ejection fraction) is <1. Therefore, for many heartbeats following inversion, some fraction of blood delivered to the myocardium will be labeled (due to circulation of inverted blood and ejection fraction<1).

To account for the blood magnetization input function in the slice-selective case, we used the modified Bloch equations presented by Detre et al., (26) describing the longitudinal magnetization with the effects of perfusion (Eq. [2]). Sufficiently fast exchange of spins between intravascular and extracellular compartments has been demonstrated by Bauer et al., (27) in rats and Wacker et al., (28) in humans, meeting the assumptions of this model. This model has been used previously to estimate cerebral perfusion in cases where the $M_{\text{blood}}(t)$ input is not straightforward (29).

$$\frac{dM_{\text{tissue}}(t)}{dt} = \frac{M_{0\text{tissue}}}{T_{1\text{tissue}}} - \left(\frac{1}{T_{1\text{tissue}}} + \frac{\text{MBF}}{\lambda}\right)M_{\text{tissue}}(t) + \text{MBF}\cdot M_{\text{blood}}(t) \quad [2]$$

$M_{\text{tissue}}(t)$ myocardial T_1 recovery curves are measured, λ is known, and $M_{\text{blood}}(t)$ curves can be approximated from the blood pool magnetization. The remaining three parameters, MBF, $T_{1\text{tissue}}$ and $M_{0\text{tissue}}$, can be determined through curve fitting to the inversion recovery Look-Locker data. Equation 2 can also be solved in the general case for any function $M_{\text{blood}}(t)$ by:

$$M_{\text{tissue}}(t) = M_{0\text{tissue}}\frac{T_{1\text{app}}}{T_{1\text{tissue}}}\left(1 - e^{\frac{-t}{T_{1\text{app}}}}\right) + M_{\text{tissue}}(0)e^{\frac{-t}{T_{1\text{app}}}} + \text{MBF}\int_0^t M_{\text{blood}}(\tau)e^{\frac{(\tau-t)}{T_{1\text{app}}}}d\tau \quad [3]$$

with $\frac{1}{T_{1\text{app}}} = \frac{1}{T_{1\text{tissue}}} + \frac{\text{MBF}}{\lambda}$

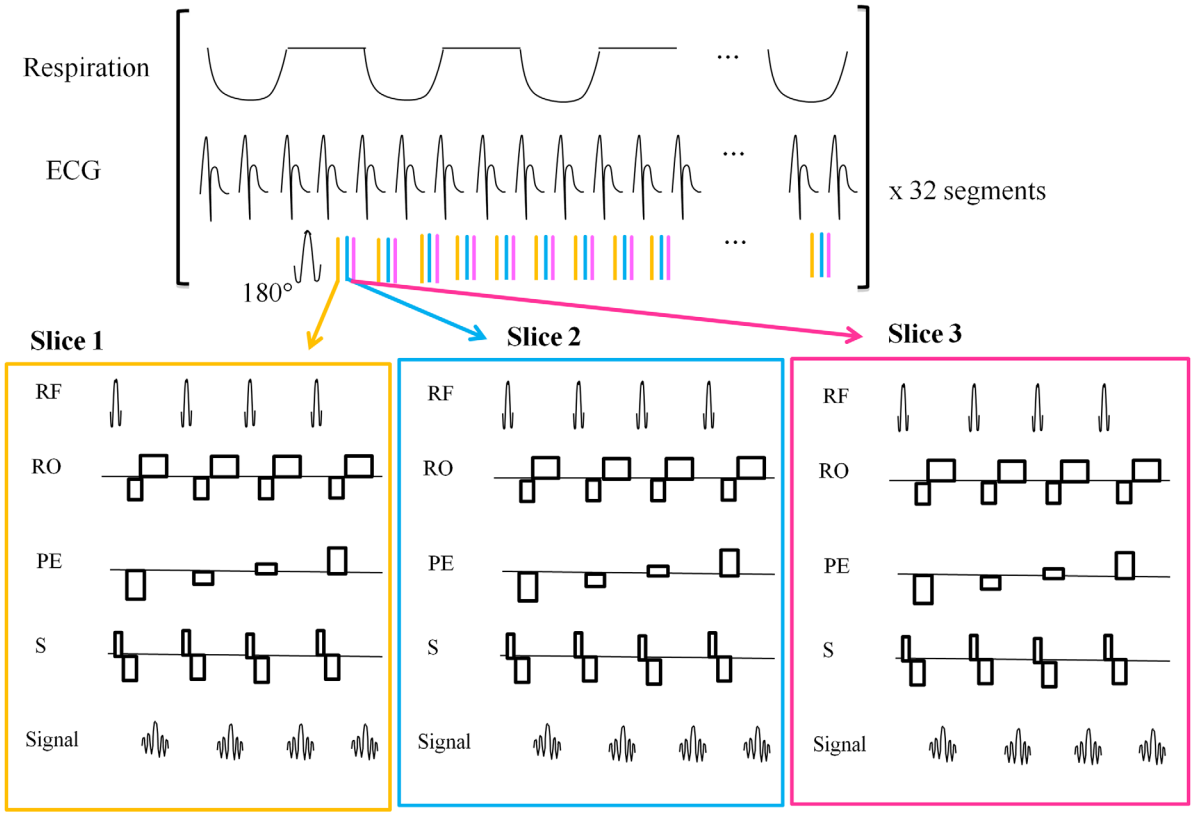

FIG. 2. Multislice T_1 mapping pulse sequence diagram. The inversion pulse is triggered to occur during the first heart beat after a breath, then for each heart beat during T_1 recovery, four lines of k-space are acquired per slice. The inversion recovery is repeated 32 times to acquire the full k-space matrix for all images. [Color figure can be viewed in the online issue, which is available at wileyonlinelibrary.com.]

For this study, we used a numerical integration of Eq. [2] for the estimation of MBF, however, Eq. [3] could also be used.

METHODS

Pulse Sequence

Data were acquired on a 9.4T Agilent scanner (Agilent Technologies, Santa Clara) with volume resonator RF coil (diameter 35 mm, length 60 mm, RAPID Biomed, Rimpar, Germany). The segmented ECG-gated Look-Locker T_1 mapping sequence (22) was extended to have multislice capabilities (Fig. 2). Four lines of k-space are acquired per heart beat for each slice (requiring 12 ms per slice acquisition), meaning each slice is acquired at a slightly different cardiac phase. Using this sequence slice-selective and global recovery curves for multiple slices can be acquired in a total acquisition time of ~15 min. We acquired three slices per acquisition at the beginning of systole in these studies (5 ms delay after R-wave trigger before acquisition). Slice-selective inversion thickness was wide enough to include all slices (at least 6 mm for three 1.5 mm slices) and global inversion thickness was set to 150 mm to cover the entire mouse. Inversion and excitation were performed using an adiabatic full passage (sech pulse, length = 4 ms, and bandwidth = 20 kHz) and gaussian pulses (length = 500 μs), respectively. A data logger (Cambridge Electronic Design, Cambridge, UK) was used to record ECG, respiration and RF events for the retrospective rejection of images deemed to be corrupted by respiration based on the central two lines of k-space. In addition, the data logger trace was used to trigger the scanner at each ECG event recorded as well as interpolate overdue RF triggers (activated after [mean +1 standard deviation RR interval] has elapsed since previous trigger), as described previously (22).

Multislice T_1 mapping was compared with single slice segmented ECG-gated Look-Locker acquisition in phantoms of 0, 0.3, 0.6, and 1.3 mM Ni^{2+} in agarose and in vivo (n =3 CD1 mice). The T_1 of three slices acquired separately was compared with the T_1 of the same slices acquired using the multislice acquisition for slice-selective and global inversion. Scan parameters were set as follows: TE/TR(inv)/TR(RF) = 1.18 ms/13.5 s/3 ms, 4 lines of k-space per heart beat, flip angle = 5°, FOV = 40 × 40 mm^2 (phantom) or 25.6 × 25.6 mm^2 (in vivo), matrix = 128 × 128, slice thickness = 1.5 mm, inversion thickness = 7.5 mm (slice-selective) or 150 mm (global), number of slices = 1 or 3, slice gap = 0 mm, number of points in recovery curve= 50, slice acquisition order = centric, short-axis view (in vivo).

bpMBF Quantification Method

$M_{blood}(t)$ Quantification

The blood magnetization input in Eq. [2] was estimated from a measurement of left ventricle blood pool magnetization at the previous heart beat with 1 RR-interval's T_1

recovery (modeled), for both slice-selective and global inversion. This blood pool is already present in the cardiac images, and therefore no extra data acquisition is necessary. We assume that the spins are well mixed and the net magnetization is measured (from hand-drawn regions of interest including entire visible blood pool). The time-varying blood magnetization curve throughout inversion recovery was compared for multiple slice-selective thicknesses and different short axis positions in vivo in six CD1 mice (not all positions/thicknesses acquired in all subjects).

Curve Fitting

Numerical integration of Eq. [2] was performed to generate $M_{\text{tissue}}(t)$ curves for given $M_{\text{blood}}(t)$ data input and the mean-squared difference between the experimental data and the synthesized $M_{\text{tissue}}(t)$ curves was minimized for slice-selective and global data simultaneously to fit for MBF, $T_{1\text{tissue}}$ and $M_{0\text{tissue}}$. Because a 5° flip angle was used, it was assumed that the effect of the Look-Locker RF train on the $M_{\text{tissue}}(t)$ curve was negligible compared with other effects. To initialize the MBF parameter value, a linear fit was used (as described in Appendix 1).

Simulations of $M_{\text{tissue}}(t)$ and bpMBF Quantification

Modeling of $M_{blood}(t)$

For the purposes of simulation, $M_{\text{blood}}(t)$ after slice-selective inversion was modeled to a first approximation by a three parameter exponential fit Eq. [4], as informed by experimental results (see Results):

$$M_{\text{blood}}(t) = M_{0\text{blood}}\left(1 - \varepsilon\, e^{\frac{-t}{T_{\text{b,ss}}}}\right) \quad [4]$$

where $T_{\text{b,ss}}$ is the time constant describing the recovery to equilibrium of the left ventricle blood after slice-selective inversion (related to pulmonary circulation, $T_{1\text{blood}}$ and ejection fraction), and ε is an indication of the initial fraction of inverted blood in the left ventricle. To model the variations in $M_{\text{blood}}(t)$ with slice-selective inversion thickness, ε was varied from $\varepsilon = 0$ (all inflowing blood is fresh) to $\varepsilon = 2$ (all blood in left-ventricle is inverted), while $T_{\text{b,ss}}$ and $M_{0\text{blood}}$ were kept constant. For global inversion, $M_{\text{blood}}(t)$ was assumed to be an exponential recovery:

$$M_{\text{blood}}(t) = M_{0\text{blood}}\left(1 - 2e^{\frac{-t}{T_{1\text{blood}}}}\right)$$

MBF and ε were varied in simulations and other parameters were fixed based on observed values as follows: $M_{0\text{tissue}} = 0.07$ au, $T_{1\text{tissue}} = 1.7$ s, $\lambda = 0.95$ mL/g, $M_{0\text{blood}} = 0.08$ au, $T_{\text{b,ss}} = 1.4$ s, and $T_{1\text{blood}} = 2$ s. For the purposes of our simulation, the numerical integration of Eq. [2] was used to mimic the in vivo quantification method. As an alternative method, Eq. [3] can be solved explicitly for simulated $M_{\text{blood}}(t)$, which gives identical $M_{\text{tissue}}(t)$ curves to numerical integration of Eq. [2] using the simulated parameters (data not shown).

Simulation Experiments

Three simulation experiments were performed. Experiment 1: Using the numerical integration of Eq. [2], $M_{\text{tissue}}(t)$ curves were generated for a variety of $M_{\text{blood}}(t)$ curves to simulate the relationship observed in vivo. Experiment 2: The mean-squared difference between synthetic $M_{\text{tissue}}(t)$ curves generated with perturbations in MBF (MBF ± 5 mL/g/min) was used to assess the sensitivity of the mean-squared difference objective function and the ability to correctly estimate MBF. Experiment 3: To test the quantification methods, global and slice-selective $M_{\text{tissue}}(t)$ curves were generated for a given MBF at a range of ε values and noise was added to the curves (100 repetitions). We compare MBF quantified using fit $T_{1\text{global}}$ and $T_{1\text{slice-selective}}$ in the standard method (Eq. [1]) to the multiparameter bpMBF quantification method. For figures, MBF = 5, 10, and 15 mL/g/min are shown, as well as MBF = 0 mL/g/min for the model comparison.

In Vivo Validation

Animal experiments were completed according to the UK Animal (Scientific Procedures) Act 1986 and local guidelines. For technique development and validation, CD1 mice were used. Anesthesia was induced with 4% isoflourane in 2 L/min O_2 and maintained at 1.5–2% isoflurane in 1 L/min O_2. A small animal physiological monitoring device (SA Instruments, Stony Brook, NY) was used to monitor respiration using a neonatal apnea pad, temperature using a rectal probe and ECG using two electrodes inserted subcutaneously.

Perfusion was estimated using standard quantification (Eq. [1]) and bpMBF quantification for the same midventricle single slice with a variety of slice-selective inversion thicknesses ($n = 5$). To compare single to multislice perfusion estimates, the mean perfusion estimates from the centre slice of a multislice acquisition were compared with single slice perfusion estimates in the same slice using bpMBF in $n = 8$ data sets. A combination of apical and midventricle positions were used, and slice-selective inversion thickness = 6 or 7.5 mm (multislice) and 4.5 mm (single slice). Multislice MBF maps are shown from one animal to demonstrate sensitivity to experimental manipulation with isoflurane varied from 1.25 to 2% (previously shown to produce a ~2.5 fold increase in perfusion (10,22)) and for comparison to single slice ASL acquisition.

RESULTS

Pulse Sequence

T_1 measurements generated using the single and multislice acquisitions compared well (Fig. 3). In phantoms, $T_{1\text{multi}} = 1.00 \cdot T_{1\text{single}} - 0.03$ s, and in vivo, $T_{1\text{multi}} = 0.77 \cdot T_{1\text{single}} + 0.37$ s. The additional variation in vivo was due to physiological noise, range of physiological T_1 values ($T_{1,\text{slice-selective}} = 1.31$–$1.50$ s and $T_{1\text{global}} = 1.78$–$1.92$ s for single slice acquisition) or subtle differences in cardiac cycle. A small bias is observed in phantom T_1 quantification where the multislice sequence overestimates T_1 by a small margin. This overestimation is a small effect compared with physiological noise in vivo.

Measurements of Blood Magnetization

In Vivo $M_{blood}(t)$ and $M_{tissue}(t)$ Curves

For a range of inversion thicknesses, we observed that the blood pool magnetization requires ~3 s to return to

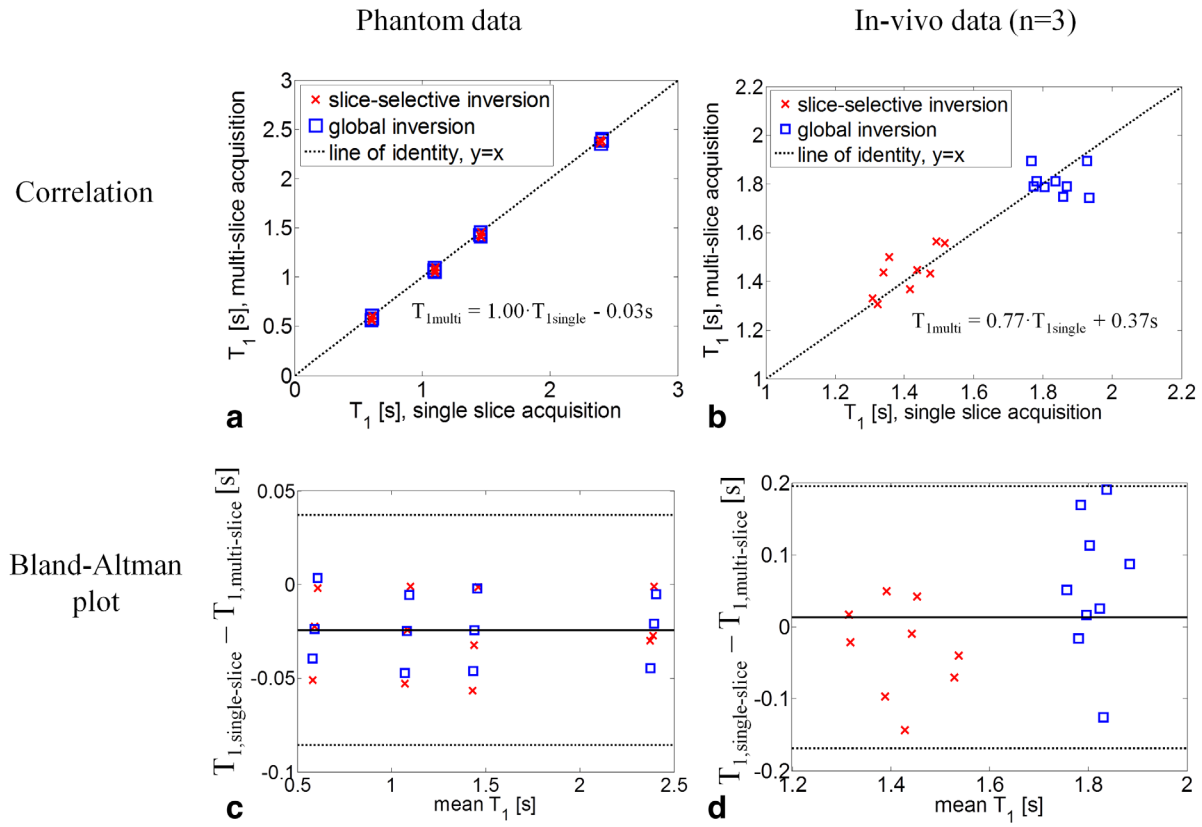

FIG. 3. Comparison of T_1 measurements generated using single and multislice acquisitions by correlation (**a**,**b**) and Bland-Altman plots (**c**,**d**). T_1 is compared in four Ni^{2+}phantoms (a,c; 0, 0.3125, 0.625, and 1.25 mM in 2% agarose) and in the myocardium (b,d; $n = 3$ CD1 mice). Three slices were acquired using multislice acquisition and compared with the T_1 of the same three slices acquired using single slice acquisition. For the Bland Altman plots, the solid line represents the mean difference in T_1 and the dotted lines represent ±1.96 standard deviations of the difference in T_1 generated from single and multislice acquisitions. For the purposes of assessing the sequence, slice-selective inversion thickness was 7.5 mm for both single and multislice acquisitions. [Color figure can be viewed in the online issue, which is available at wileyonlinelibrary.com.]

equilibrium in the left ventricle (Fig. 4). The amount of blood inverted increases with slice-selective inversion thickness, as expected, and with midventricle positioning. Slice-selective tissue magnetization recovery curves become closer to global recovery curves as the amount of inverted blood increases.

Modeling Parameters of $M_{blood}(t)$

Parameter ε (Eq. [3]) demonstrated a clear positive relationship with the slice-selective thickness (Fig. 5). However, $T_{b,ss}$ and M_{0blood} are not strongly related to slice-selective thickness. The relationship (slope and R^2) between the parameters and slice-selective thickness are given in Table 1. This justified our choice to vary ε and keep M_{0blood} and $T_{b,ss}$ constant for the purpose of $M_{blood}(t)$ simulation. ε takes a lower value when slices are positioned closer to the apex because less blood is inverted in this case. $M_{blood}(t)$ parameters were found to be independent of isoflourane levels (data in Supporting Information). Typical values of ε for a midventricle slice are 0.75−1 for single-slice inversion thicknesses (blue curve in Fig. 4) and 1.25–1.5 for multislice inversion thicknesses (red curve in Fig. 4).

Simulations of $M_{tissue}(t)$ and bpMBF Quantification

Experiment 1: Varying the simulated shape of $M_{blood}(t)$ confirmed a relationship with $M_{tissue}(t)$ (Fig. 6), which was analogous to the in vivo data shown in Figure 4. Experiment 2: For larger values of ε (and thus wider slice-selective thickness) or for higher MBF, the mean-squared difference curve is flatter and the minimum is more difficult to detect, meaning MBF values are more difficult to estimate correctly (Fig. 7). For example, when ε = 2 the slice-selective inversion recovery curves are very similar to the global inversion recovery curves, making the estimation of MBF challenging. This is an important observation relevant to planning the position of slices and inversion thickness used.

Experiment 3: Simulations show that when the assumptions of Eq. [1] are satisfied (ε = 0) or if MBF = 0 mL/g/min, the MBF is correctly estimated, otherwise, the standard quantification method (Eq. [1]) underestimates MBF, particularly if ε > 0.5 (Fig. 8a). However, using bpMBF quantification, MBF is well estimated regardless of ε (Fig. 8b). As ε increases, the uncertainty of the bpMBF estimation increases, as predicted above. This simulation indicates that the bpMBF quantification method is better suited to the estimation of myocardial

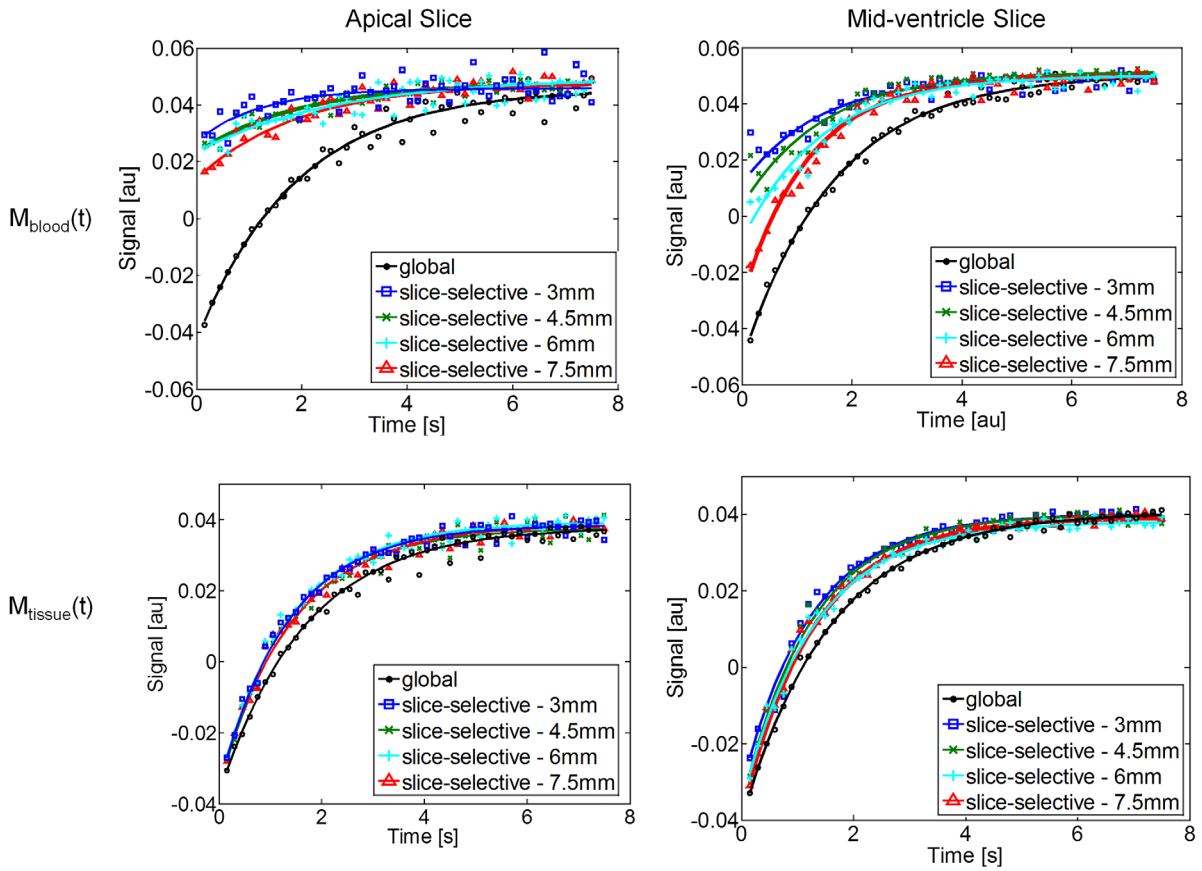

FIG. 4. Blood pool and tissue magnetization curves from one animal plotted throughout the inversion recovery sequence generated from single slice acquisitions with varying slice-selective inversion thickness. Blood pool magnetization measurement is taken from a region of interest in the left ventricle. This shows the raw time-varying blood magnetization and its relationship to slice-selective thickness and slice position. As slice-selective inversion thickness increases and more blood is inverted, the tissue magnetization curve becomes more similar to the global magnetization curve. In some cases, the changes in tissue magnetization curves are very subtle and curves are therefore overlaid in the plot. Three parameter curve fits are also plotted. [Color figure can be viewed in the online issue, which is available at wileyonlinelibrary.com.]

perfusion under realistic circumstances, recalling the typical values of ε from the in vivo data were 0.75−1 for single slice inversion thickness and 1.25−1.5 for multislice inversion thickness.

In Vivo Validation

Mean MBF estimates from the standard quantification method (Eq. [1]) show a negative trend with slice-selective inversion thickness (Fig. 9a) for the same midventricle slice. The mean [95% confidence interval] slope of this relationship was −1.17 mL/g/min/mm (−1.95 mL/g/min/mm − 0.39 mL/g/min/mm) and $R^2 = 0.72$. Importantly, the bpMBF quantification generates more consistent MBF estimates for the same data sets (Fig. 9b), with a group mean [95% confidence interval] slope of 0.02 mL/g/min/mm (−1.13 mL/g/min/mm, 1.16 mL/g/min/mm) and $R^2 = 0.37$. This matches the simulation predictions well. The mean coefficient of variation (30) of the MBF estimates is 21%, which is within the expected range of within-session variability of the single slice technique found previously (22).

Comparing myocardial perfusion estimates from the central slice of multislice acquisitions to single slice acquisition of the same slice using bpMBF quantification gave a mean coefficient of variation of 16% (n =8 measurements). This is within the expected range of the within-session variability found previously (22), indicating the good correspondence between measurements. Figure 10 shows MBF maps (generated using bpMBF quantification) of three contiguous midventricle slices acquired using multislice ASL demonstrating increased perfusion with increased isoflurane levels. In addition, multislice MBF maps show good correspondence to single slice MBF maps acquired of the same three slices.

DISCUSSION AND CONCLUSIONS

To summarize, we have developed a multislice ECG-gated Look-Locker T_1 mapping pulse sequence together with a new method for quantifying MBF by ASL. We demonstrated that the bpMBF quantification method is more robust to variations in the slice-selective inversion thickness than standard quantification methods, and is ideally suited to multislice ASL data. This new methodology has been used to generate multislice perfusion maps in vivo in the mouse heart.

Pulse Sequence

The multislice T_1 mapping pulse sequence presented here is an extension of the single slice sequence

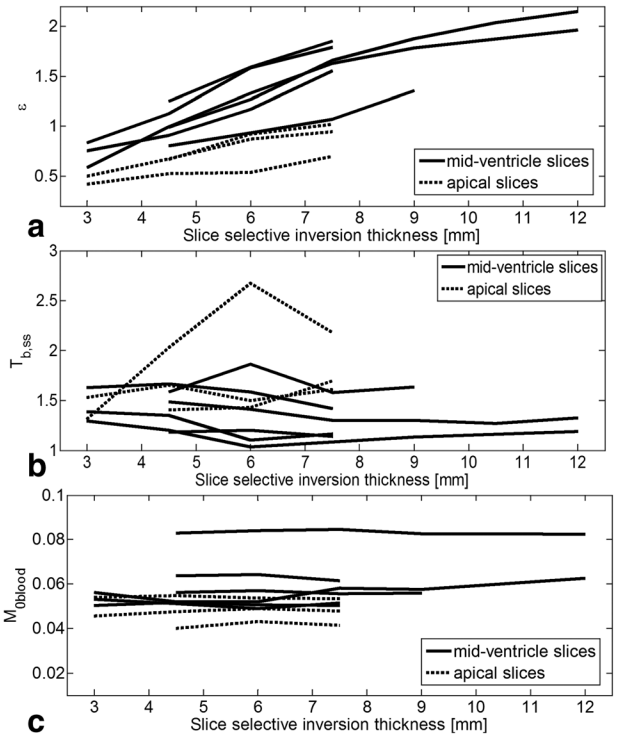

FIG. 5. Parameters of $M_{blood}(t)$ exponential curve fit (**a**) ε, (**b**) $T_{b,ss}$, and (**c**) M_{0blood} from 6 CD1 mice scanned at a variety of slice-selective inversion thicknesses and positions. Data from individual animals are plotted using solid lines for midventricle slices and dotted lines for apical slices. There is a clear positive relationship between ε and slice-selective inversion thickness, whereas $T_{b,ss}$ and M_{0blood} are constant with slice-selective inversion thickness. This justifies our choice to vary ε and keep $T_{b,ss}$ and M_{0blood} constant when modeling slice-selective $M_{blood}(t)$ for simulation purposes.

Table 1
Relationship Between $M_{blood}(t)$ Parameters and Slice-Selective Thickness (Fig. 5) Given by Slope and R^2

	Mean slope (95% confidence interval)	R^2
ε	0.17 mm^{-1} [0.13 mm^{-1}, 0.21 mm^{-1}] (mid ventricles slices)	0.96
	0.09 mm^{-1} [0.01 mm^{-1}, 0.17 mm^{-1}] (apical slices)	0.94
$T_{b,ss}$	0.02 s/mm [−0.05 s/mm, 0.08 s/mm]	0.44
M_{0blood}	$2.72 \cdot \times 10^{-5}$au/mm [$-3.91 \cdot \times 10^{-4}$ au/mm, $4.45 \cdot \times 10^{-4}$ au/mm]	0.44

There is a clear positive relationship between ε and slice-selective inversion thickness, whereas, $T_{b,ss}$ and M_{0blood} are constant (95% confidence interval of slope surrounds zero).

demonstrated previously (22) and was confirmed to generate accurate T_1 measurements in phantoms and in vivo. A small bias was observed in the T_1 quantification in phantoms, where multislice T_1 values were longer than single slice measurements. The magnitude of the bias depends on the acquisition order, such that the bias increases for slices acquired later in the multislice acquisition. This is likely because the slice gap is set to 0 mm and therefore the excitation pulses will affect the magnetization of the neighboring slices. In vivo, the mean difference in T_1 is approximately zero (combining global and slice-selective inversion data sets); however, a slight negative bias still appears to be present in the slice-selective case. The magnitude of this bias is very small (compared with physiological variation) and should not significantly affect results.

We chose to acquire four lines of k-space per heart beat per slice in order to ensure limited cardiac motion during the acquisition for each slice. Each k-space segment requires a 12 ms acquisition, and therefore the three slices will be acquired at slightly different cardiac phases. Although full heart coverage is ideal, three slices is advantageous over a single slice, particularly in regional conditions such as myocardial infarction. A different number of slices could be acquired with the same sequence depending on the needs of the study; however, decreased fitting sensitivity with larger volumes of inverted blood after slice-selective inversion must be

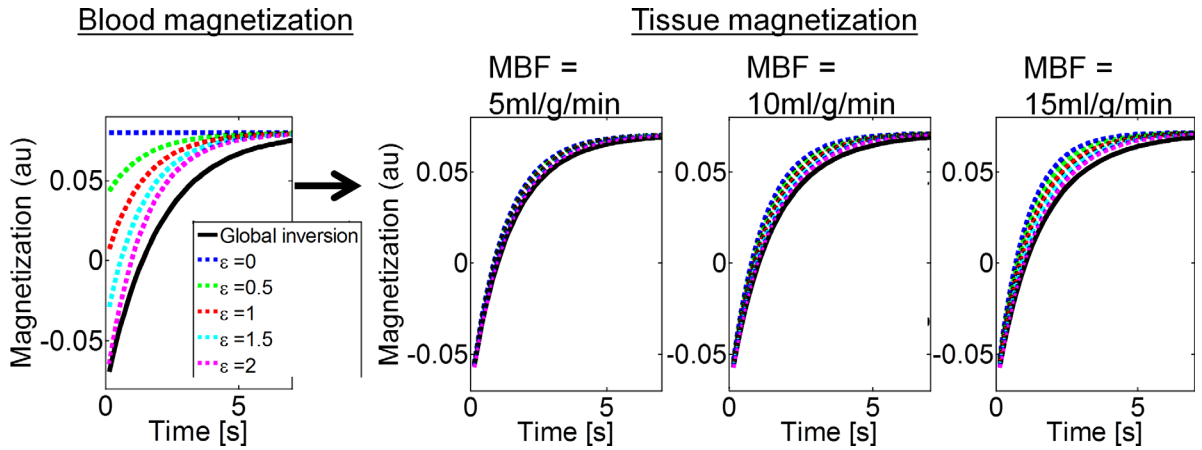

FIG. 6. Simulated slice-selective $M_{blood}(t)$ curves generated by varying ε (ε = 0, 0.5, 1, 1.5, and 2), and global $M_{blood}(t)$ curve are shown on the left hand side. The resulting tissue magnetization curves generated using Eq. [2] for a range of MBF values are shown on the right hand side. Simulated variations in $M_{blood}(t)$ have the expected effect on $M_{tissue}(t)$. [Color figure can be viewed in the online issue, which is available at wileyonlinelibrary.com.]

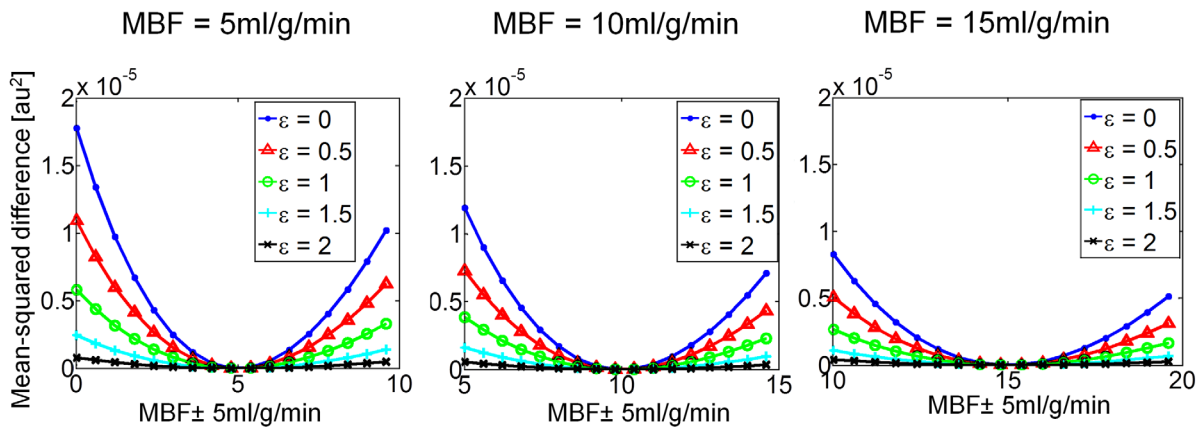

FIG. 7. Mean-squared difference between $M_{tissue}(t)$ curves for perturbations in MBF, indicating the ability to accurately find the experimental MBF. It was observed that the mean-squared difference curve is flatter with increased ε and higher MBF, meaning the correct MBF is more difficult to estimate. [Color figure can be viewed in the online issue, which is available at wileyonlinelibrary.com.]

considered. If full heart coverage is required, we would recommend two acquisitions of three 1.5 mm slices (30 min acquisition time, 9 mm coverage). It is also important to note that perfusion will change throughout the cardiac cycle, as coronary blood flow is highest during diastole, and this may introduce a small slice differences to perfusion values (31).

Alternatively, the same temporal resolution for the acquisition of three slices could be achieved by acquiring 12 lines of k-space per cardiac cycle and performing three separate single slice acquisitions. This may introduce blurring due to myocardial motion as the segment of k-space is acquired over 36 ms. Therefore, there is a trade-off between thicker slice-selective inversions or myocardial blurring. We believe that acquiring a limited number of slices per acquisition with a restricted slice-selective inversion thickness is better than introducing myocardial blurring.

bpMBF Quantification Method

This study has demonstrated that perfusion can be underestimated when making incorrect assumptions about the blood magnetization input function, particularly in the multislice case. This effect has not previously been investigated in detail in the heart. Our in vivo blood pool magnetization plots (Fig. 4) show that even for the thinnest slice-selective thickness (3 mm), the blood magnetization is not at equilibrium at short inflow times, indicating that perfusion could potentially be misestimated even in the single slice case. The slice-selective inversion thickness must be wider than the imaging slice to compensate for slice profile effects. Particularly when investigating a midventricle slice, the slice-selective inversion thickness necessary for multislice acquisition (at least 6 mm for 3 contiguous 1.5 mm slices) results in a large fraction of inverted blood. These

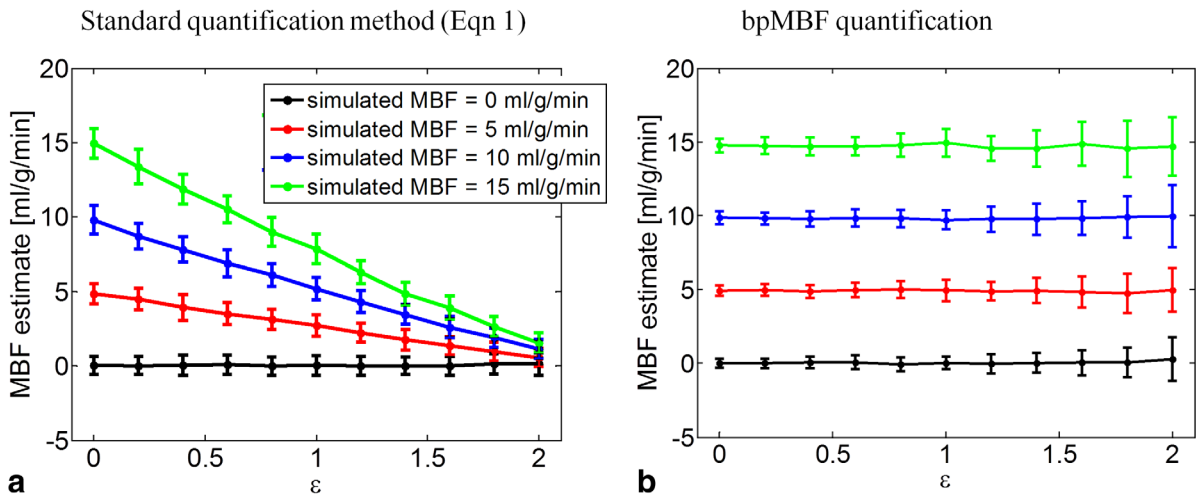

FIG. 8. Simulated perfusion quantification using (**a**) standard quantification (Eq. [1]) and (**b**) bpMBF for a range of inversion thicknesses (ε) and MBF values 0, 5, 10, and 15 mL/g/min. Each point represents the mean ± standard deviation perfusion estimate generated for 100 repetitions of the simulation with noise added to recovery curves. The standard quantification method (Eq. [1]) underestimates perfusion particularly for wide slice-selective inversion (high ε) and high MBF values. The bpMBF quantification method accurately estimates perfusion in all cases. [Color figure can be viewed in the online issue, which is available at wileyonlinelibrary.com.]

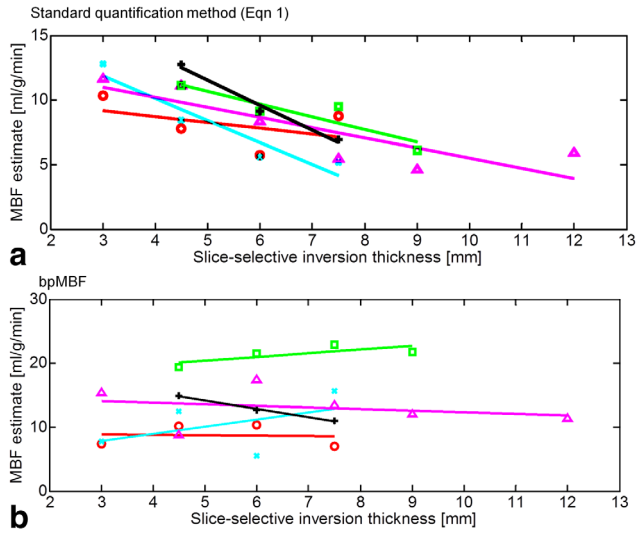

FIG. 9. MBF estimates from (**a**) standard quantification method (Eq. [1]) and (**b**) bpMBF quantification for the same midventricle single slice with varying slice-selective inversion thickness in 5 CD1 mice (each represented by a different color), and their linear fits. It is found that the bpMBF method generates a more consistent perfusion estimate for all slice-selective inversion thicknesses; whereas estimated MBF decreases with slice-selective thickness using Eq. [1].

effects are much less of a concern in other organs where the volume of inverted blood is much lower.

The novelty of this MBF quantification method comes from the direct measurement of the blood magnetization from the left-ventricle blood pool at each time point of the Look-Locker T_1 acquisition in vivo. This method makes no assumptions about the blood magnetization at any point in the MBF quantification. Here we have focused on slice-selective inversion thickness, however other factors, such as impaired cardiac function, may also change the blood magnetization input function. This should not affect MBF quantification because blood magnetization is directly measured for each case. In addition, this method is not reliant on assumptions of blood T_1, which reduces the sensitivity of perfusion measurements to blood oxygenation. In the future, a more comprehensive model of the blood magnetization, such as recently presented by Kampf et al. (32), may be useful.

It was assumed for the bpMBF quantification method that the Look-Locker saturation (using a flip angle of 5°) had a minimal effect on the T_1 curves compared to the blood magnetization and perfusion. If, however, a different implementation requires this effect to be considered, an iterative updated fitting process could be used at the cost of extra computation time.

$T_{1\text{tissue}}$ was a fitted parameter, rather than assumed to be equal to $T_{1\text{global}}$, because this assumption is not valid at the high perfusion rates present in the mouse heart (as validated by simulation, not shown) and will lead to a misestimation of perfusion. Therefore, we chose to perform a fit with three free parameters: $M_{0\text{tissue}}$, $T_{1\text{tissue}}$, and MBF. The linear fit used to initialize the MBF parameter, shown in Appendix 1, was an original approach to estimating MBF. It is, however, not as sensitive as the three parameter fit.

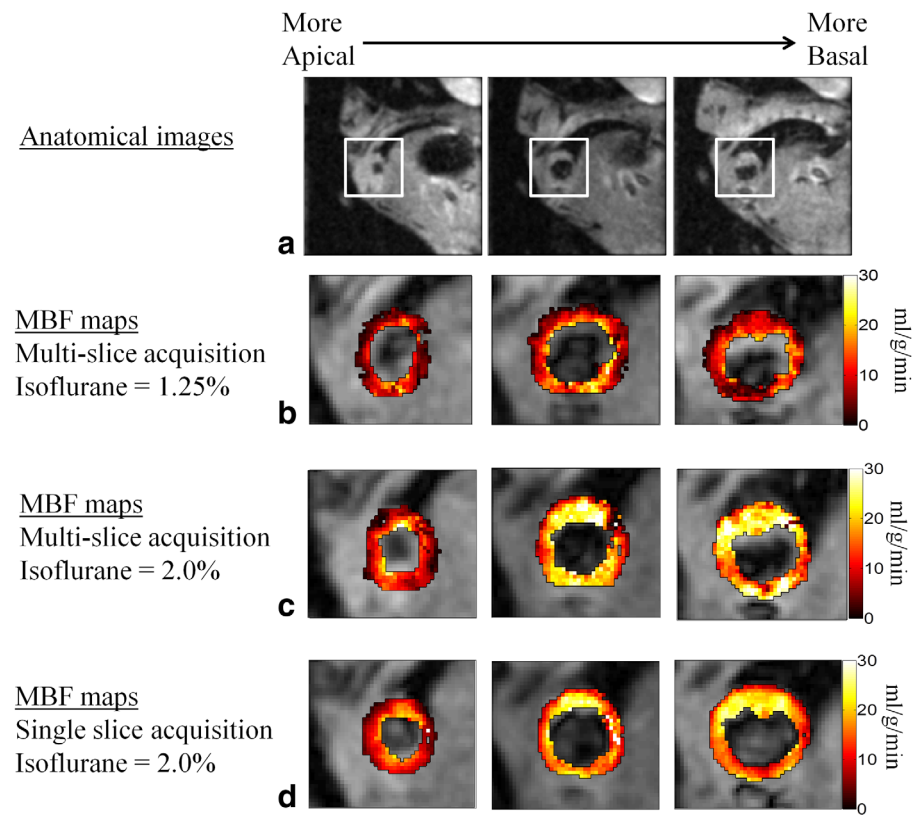

FIG. 10. (**a**) Anatomical images from multislice Look-Locker acquisition of three contiguous midventricle slices, (**b**) multislice MBF maps overlaid on anatomical images with isoflurane = 1.25%, (**c**) multislice MBF maps with isoflurane = 2%, and (**d**) single slice MBF maps of same three contiguous slices acquired with isoflurane = 2%. For multislice and single slice acquisitions, slice-selective inversion thickness was 7.5 and 4.5 mm, respectively. The multislice images were acquired in the following order: centre slice, more apical slice, and more basal slice. Increased isoflurane results in increased MBF, particularly in the more basal two slices. A good agreement between single and multislice acquisition is observed in MBF maps.

Simulations of $M_{tissue}(t)$ and bpMBF Quantification

Simulations calculating the difference between tissue magnetization curves for small perturbations in MBF (Experiment 2) showed the importance of minimizing ε to enable accurate identification of the minimum of the objective function. Maximizing the difference between the slice-selective and global recovery curves improves the ability to fit the data and correctly estimate MBF. In order to do this, one must minimize the amount of blood inverted in the slice-selective case by: acquiring a fewer number of slices and doing extra acquisitions to cover the area of interest, if necessary; minimizing the inversion thickness; positioning the slices near the apex; or, choosing an inversion plane different to imaging plane, as long as myocardial tissue is included. It is important to be aware that errors may be introduced into perfusion for wider slice-selective thicknesses and high perfusion rates.

Simulations estimating MBF using the standard method (Eq. [1]) and bpMBF showed the underestimation of perfusion using Eq. [1] under certain conditions (Experiment 3). Parameters for this simulation were chosen based on myocardial tissue parameters, but the MBF estimates of Eq. [1] may vary from the choice of different tissue parameters. Belle et al., (4) clearly states that the model assumes that all inflowing blood is at equilibrium in the slice-selective case, and there is the potential to underestimate perfusion if this assumption is not met. One must be careful to use this model only when appropriate, and otherwise, particularly in the multislice acquisition case, move to a model compensated for time-varying blood magnetization such as the bpMBF method.

In Vivo Validation

In vivo experiments show the robust nature of the bpMBF quantification method to changes in slice-selective inversion thickness. In contrast, the perfusion estimate generated using the standard method (Eq. [1]) decreased with increasing inversion thickness (as the assumptions of the model were increasingly invalid). The average coefficient of variation of the bpMBF perfusion estimations was slightly higher than the average within-session variability, although still within the range reported for normal animals previously (22). The increased variability could be caused by the difficulty of fitting data sets with wider slice-selective thicknesses. Importantly, the mean myocardial perfusion was found to compare well for the same slice acquired using single and multislice acquisition. The MBF maps demonstrated the sensitivity of the multislice technique to changes in perfusion. In addition, the MBF maps demonstrated the good correspondence between maps generated using single and multislice acquisitions, with small differences caused by inherent technique variability and differences in cardiac cycle.

The perfusion values generated in vivo using bpMBF quantification were of similar magnitude to those generated using Eq. [1] with the narrowest slice-selective inversion thickness within this study. Although, these values were slightly higher than those previously reported [4–7 mL/g/min (9,10,21)], which could be due to previous underestimated perfusion with Eq. [1]. In addition, anesthetic can strongly influence myocardial perfusion and therefore, it is difficult to directly compare quantitative values between studies using different anesthetic protocols.

CONCLUSION

In this study, we have presented a multislice segmented ECG-gated Look-Locker T_1 mapping sequence for application to multislice ASL perfusion measurements. We have presented a new quantification method, bpMBF, needed to accurately quantify the multislice ASL signal, which uses an estimation of the blood magnetization from the left ventricle blood pool. We demonstrated though simulation that perfusion estimation using this method is robust to changes in slice-selective thickness, and furthermore suggest that the bpMBF quantification method may be more applicable under realistic conditions, particularly for multislice acquisition. The ability to acquire multislice perfusion data in a single acquisition will be of great benefit to the study of cardiac disease and the techniques presented here will be of much use in future cardiac MRI studies.

APPENDIX

In this study, a multiparameter fit was used to generate MBF estimates. The MBF parameter of this fit was initialized using the linear fit described here. The Bloch equations modified to including perfusion give:

$$\frac{dM_{tissue}(t)}{dt} = \frac{M_{0tissue}}{T_{1tissue}} - \left(\frac{1}{T_{1tissue}} + \frac{MBF}{\lambda}\right) M_{tissue}(t) + MBF \cdot M_{blood}(t) \quad [A1]$$

Following the structure of the Look-Locker acquisition, Eq. [A1] can be considered at time points, t_i, one RR-interval apart:

$$M'_{tissue}(t_i) = \frac{M_{0tissue}}{T_{1tissue}} - \left(\frac{1}{T_{1tissue}} + \frac{MBF}{\lambda}\right) M_{tissue}(t_i) + MBF \cdot M_{blood}(t_i) \quad [A2]$$

The notation M'_{tissue} is used for the temporal derivative. For n points on Look-Locker recovery curve, t_i takes values t_1 to t_n.

Calculating $M_{blood}(t_i)$

The magnetization of the blood perfusing into the myocardium is best modeled as the left-ventricle blood pool magnetization during the previous heart beat having one RR-interval (length of time defined as RR) of T_1 magnetization recovery. From the general solution to the Bloch equations, T_1 recovery can be described by: $M(t) = M_0 + [M(0) - M_0] \exp(-t/T_1)$. Therefore, $M_{blood}(t_i)$ can be rewritten as follows:

$$M_{blood}(t_i) = M_{0blood} + [M_{bloodpool}(t_{i-1}) - M_{0blood}] \exp(-RR/T_{1blood}) \quad [A3]$$

where $M_{bloodpool}(t_{i-1})$ is a measured value. Substituting Eq. [A3] into Eq. [A2] for $M_{blood}(t_i)$ gives:

$$M'_{\text{tissue}}(t_i) = \frac{M_{0\text{tissue}}}{T_{1\text{tissue}}} - \left(\frac{1}{T_{1\text{tissue}}} + \frac{\text{MBF}}{\lambda}\right) M_{\text{tissue}}(t_i) + \text{MBF} \cdot \left[M_{0\text{blood}} + [M_{\text{bloodpool}}(t_{i-1}) - M_{0\text{blood}}] \exp(-RR/T_{1\text{blood}})\right] \quad [A4]$$

Numerical coefficients of Eq. [A4] can be grouped to simplify notation to:

$$M'_{\text{tissue}}(t_i) = \beta 0 + \beta 1 \cdot M_{\text{tissue}}(t_i) + \beta 2 \cdot M_{\text{bloodpool}}(t_{i-1}) \quad [A5]$$

With coefficients:

$$\vec{\beta} = \begin{pmatrix} \beta 0 \\ \beta 1 \\ \beta 2 \end{pmatrix} = \begin{pmatrix} \frac{M_{0\text{tissue}}}{T_{1\text{tissue}}} + \text{MBF} \cdot M_{0\text{blood}}(1 - \exp(-RR/T_{1\text{blood}})) \\ -\left[\frac{1}{T_{1\text{tissue}}} + \frac{\text{MBF}}{\lambda}\right] \\ \text{MBF} \cdot \exp(-RR/T_{1\text{blood}}) \end{pmatrix}$$

For ASL measurement, magnetization is measured after a global and a slice-selective inversion, we therefore have two equations both satisfied by the same coefficients $\vec{\beta}$

$$M'_{\text{tissue,global}}(t_i) = \beta 0 + \beta 1 \cdot M_{\text{tissue,global}}(t_i) + \beta 2 \cdot M_{\text{bloodpool,global}}(t_{i-1})$$

and

$$M'_{\text{tissue,slice-selective}}(t_i) = \beta 0 + \beta 1 \cdot M_{\text{tissue,slice-selective}}(t_i) + \beta 2 \cdot M_{\text{bloodpool,slice-selective}}(t_{i-1})$$

This linear system can be solved for $\vec{\beta}$ using measured magnetization vectors $M_{\text{tissue}}(t_i)$ and $M_{\text{bloodpool}}(t_{i-1})$, and $M'_{\text{tissue}}(t_i)$ estimated as follows, considering each of these vectors to contain both slice-selective and global inversion recovery data.

Calculating $M'_{\text{tissue}}(t_i)$

$M'_{\text{tissue}}(t_i)$ could be calculated using numerical finite differences in $M_{\text{tissue}}(t_i)$; however, we found that using the $M_{\text{tissue}}(t)$ fit parameters as follows provided a more stable solution. The tissue magnetization experimental data from the global and slice-selective inversion recoveries are typically modeled as a three parameter exponential:

$$M_{\text{tissue}}(t) = M_{0\text{tissue}} \cdot (1 - \alpha \exp(-t/T_1*))$$

where T_1* is the effective T_1 before Look-Locker correction and α is the inversion efficiency. Therefore, $M'_{\text{tissue}}(t_i)$ can be calculated from slice-selective and global inversion recovery curves using the curve fit parameters:

$$M'_{\text{tissue}}(t) = \frac{M_{0\text{tissue}} \cdot \alpha}{T_1*} \exp(-t/T_1*)$$

Solving For $\vec{\beta}$

The numerical coefficients of $\vec{\beta}$ can be computed by solving the linear system of Eq. [A5] with the given vectors $M_{\text{tissue}}(t_i)$, $M_{\text{bloodpool}}(t_{i-1})$ and $M'_{\text{tissue}}(t_i)$ from slice-selective and global inversion measurements. Eq. [A5] can be redefined as:

$$\vec{Y} = \mathbf{X} \bullet \vec{\beta} \quad [A6]$$

With $\vec{Y} = \begin{pmatrix} M'_{\text{tissue,global}}(t_2) \\ M'_{\text{tissue,global}}(t_3) \\ \vdots \\ M'_{\text{tissue,global}}(t_n) \\ M'_{\text{tissue,slice-selective}}(t_2) \\ M'_{\text{tissue,slice-selective}}(t_3) \\ \vdots \\ M'_{\text{tissue,slice-selective}}(t_n) \end{pmatrix}$ *and*

$$\mathbf{X} = \begin{pmatrix} 1 & M_{\text{tissue,global}}(t_2) & M_{\text{blood,global}}(t_1) \\ 1 & M_{\text{tissue,global}}(t_3) & M_{\text{blood,global}}(t_2) \\ \vdots & \vdots & \vdots \\ 1 & M_{\text{tissue,global}}(t_n) & M_{\text{blood,global}}(t_{n-1}) \\ 1 & M_{\text{tissue,slice-selective}}(t_2) & M_{\text{blood,slice-selective}}(t_1) \\ 1 & M_{\text{tissue,slice-selective}}(t_3) & M_{\text{blood,slice-selective}}(t_2) \\ \vdots & \vdots & \vdots \\ 1 & M_{\text{tissue,slice-selective}}(t_n) & M_{\text{blood,slice-selective}}(t_{n-1}) \end{pmatrix}$$

Equation [A6] is solvable for numerical coefficients $\vec{\beta}$ (1×3) using the following matrix solution:

$$\vec{\beta} = (\mathbf{X}^T\mathbf{X})^{-1}(\mathbf{X}^T\mathbf{Y}) \quad [A7]$$

To adapt for the measurement of $M_{\text{bloodpool}}$ at t_{i-1} and M_{tissue} at t_i, only $(n - 1)$ points of the Look-Locker curve are used. $M_{\text{tissue}}(t_i)$, $M_{\text{bloodpool}}(t_{i-1})$ and $M'_{\text{tissue}}(t_i)$ vectors contain both slice-selective and global Look-Locker data and have dimensions $[1 \times 2\ (n - 1)]$. Therefore, $\vec{Y}$ is a $[1 \times 2\ (n - 1)]$ vector and $\mathbf{X}$ is a $[3 \times 2\ (n - 1)]$ matrix.

Calculating MBF

Each of the coefficients in $\vec{\beta}$ can be rearranged algebraically to estimate MBF assuming values for the other parameters ($T_{1\text{tissue}}$, $T_{1\text{blood}}$, $M_{0\text{tissue}}$, or $M_{0\text{blood}}$). Because, we can estimate $T_{1\text{blood}}$ more accurately than $M_{0\text{tissue}}$ or $T_{1\text{tissue}}$, we chose to use $\beta 2$to generate an estimate of MBF. Blood pool estimation of $T_{1\text{blood}}$ from the global Look-Locker curve was used to estimate MBF from the following relationship:

$$\text{MBF} = \beta_2 \cdot \exp(RR/T_{1\text{blood}})$$

This MBF estimation was used as the starting value for the multiparameter fit.

REFERENCES

1. Price AN, Cheung KK, Cleary JO, Campbell AE, Riegler J, Lythgoe MF. Cardiovascular magnetic resonance imaging in experimental models. Open Cardiovasc Med J 2010;4:278–292.
2. Vallée JP, Ivancevic MK, Nguyen D, Morel DR, Jaconi M. Current status of cardiac MRI in small animals. MAGMA 2004;17:149–156.
3. Petersen E, Zimine I, Ho Y, Golay X. Non-invasive measurement of perfusion: a critical review of arterial spin labelling techniques. Br J Radiol 2006;79:688–701.
4. Belle V, Kahler E, Waller C, Rommel E, Voll S, Hiller K, Bauer W, Haase A. In vivo quantitative mapping of cardiac perfusion in rats

using a noninvasive MR spin-labeling method. J Magn Reson Imaging 1998;8:1240–1245.
5. Iltis I, Kober F, Desrois M, Dalmasso C, Lan C, Portha B, Cozzone P, Bernard M. Defective myocardial blood flow and altered function of the left ventricle in type 2 diabetic rats: a noninvasive in vivo study using perfusion and cine magnetic resonance imaging. Invest Radiol 2005;40:19–26.
6. Iltis I, Kober F, Dalmasso C, Lan C, Cozzone P, Bernard M. In vivo assessment of myocardial blood flow in rat heart using magnetic resonance imaging: effect of anesthesia. J Magn Reson Imaging 2005;22: 242–247.
7. Iltis I, Kober F, Dalmasso C, Cozzone P, Bernard M. Noninvasive characterization of myocardial blood flow in diabetic, hypertensive, and diabetic-hypertensive rats using spin-labeling MRI. Microcirculation 2005;12:607–614.
8. Jacquier A, Kober F, Bun S, Giorgi R, Cozzone PJ, Bernard M. Quantification of myocardial blood flow and flow reserve in rats using arterial spin labeling MRI: comparison with a fluorescent microsphere technique. NMR Biomed 2011;24:1047–1053.
9. Kober F, Iltis I, Izquierdo M, Desrois M, Ibarrola D, Cozzone P, Bernard M. High-resolution myocardial perfusion mapping in small animals in vivo by spin-labeling gradient-echo imaging. Magn Reson Med 2004;51:62–67.
10. Kober F, Iltis I, Cozzone P, Bernard M. Myocardial blood flow mapping in mice using high-resolution spin labeling magnetic resonance imaging: influence of ketamine/xylazine and isoflurane anesthesia. Magn Reson Med 2005;53:601–606.
11. Nahrendorf M, Hiller K, Theisen D, et al. Effect of transmyocardial laser revascularization on myocardial perfusion and left ventricular remodeling after myocardial infarction in rats. Radiology 2002;225:487–493.
12. Streif J, Hiller K, Waller C, Nahrendorf M, Wiesmann F, Bauer W, Rommel E, Haase A. In vivo assessment of absolute perfusion in the murine skeletal muscle with spin labeling MRI. Magnetic resonance imaging. J Magn Reson Imaging 2003;17:147–152.
13. Streif J, Nahrendorf M, Hiller K, Waller C, Wiesmann F, Rommel E, Haase A, Bauer W. In vivo assessment of absolute perfusion and intracapillary blood volume in the murine myocardium by spin labeling magnetic resonance imaging. Magn Reson Med 2005;53:584–592.
14. Waller C, Kahler E, Hiller K, Hu K, Nahrendorf M, Voll S, Haase A, Ertl G, Bauer W. Myocardial perfusion and intracapillary blood volume in rats at rest and with coronary dilatation: MR imaging in vivo with use of a spin-labeling technique. Radiology 2000;215:189–197.
15. Waller C, Hiller K, Voll S, Haase A, Ertl G, Bauer W. Myocardial perfusion imaging using a non-contrast agent MR imaging technique. Int J Cardiovasc Imaging 2001;17:123–132.
16. Waller C, Hiller K, Kahler E, Hu K, Nahrendorf M, Voll S, Haase A, Ertl G, Bauer W. Serial magnetic resonance imaging of microvascular remodeling in the infarcted rat heart. Circulation 2001;103:1564–1569.
17. Waller C, Engelhorn T, Hiller K, Heusch G, Ertl G, Bauer W, Schulz R. Impaired resting perfusion in viable myocardium distal to chronic coronary stenosis in rats. Am J Physiol Heart Circ Physiol 2005;288: H2588–H2593.
18. Waller C, Hiller K, Rüdiger T, Kraus G, Konietzko C, Hardt N, Ertl G, Bauer W. Noninvasive imaging of angiogenesis inhibition following nitric oxide synthase blockade in the ischemic rat heart in vivo. Microcirculation 2005;12:339–347.
19. Waller C, Hiller K, Pfaff D, Gattenlöhner S, Ertl G, Bauer W. Functional mechanisms of myocardial microcirculation in left ventricular hypertrophy: a hypothetical model of capillary remodeling post myocardial infarction. Microvasc Res 2008;75:104–111.
20. Vandsburger M, French B, Helm P, Roy R, Kramer C, Young A, Epstein F. Multi-parameter in vivo cardiac magnetic resonance imaging demonstrates normal perfusion reserve despite severely attenuated beta-adrenergic functional response in neuronal nitric oxide synthase knockout mice. Eur Heart J 2007;28:2792–2798.
21. Vandsburger M, Janiczek R, Xu Y, French B, Meyer C, Kramer C, Epstein F. Improved arterial spin labeling after myocardial infarction in mice using cardiac and respiratory gated look-locker imaging with fuzzy C-means clustering. Magn Reson Med 2010;63:648–657.
22. Campbell-Washburn AE, Price AN, Wells JA, Thomas DL, Ordidge RJ, Lythgoe MF. Cardiac arterial spin labeling using segmented ECG-gated Look-Locker FAIR: variability and repeatability in preclinical studies. Magn Reson Med 2013;69:238–247.
23. Bauer WR, Hiller KH, Roder F, Rommel E, Ertl G, Haase A. Magnetization exchange in capillaries by microcirculation affects diffusion-controlled spin-relaxation: a model which describes the effect of perfusion on relaxation enhancement by intravascular contrast agents. Magn Reson Med 1996;35:43–55.
24. Deichmann R, Haase A. Quantification of T1 Values by SNAPSHOT-FLASH NMR Imaging. J Magn Reson 1992;96:608–612.
25. Sonobe T, Schwenke DO, Pearson JT, Yoshimoto M, Fujii Y, Umetani K, Shirai M. Imaging of the closed-chest mouse pulmonary circulation using synchrotron radiation microangiography. J Appl Physiol 2011;111:75–80.
26. Detre JA, Leigh JS, Williams DS, Koretsky AP. Perfusion imaging. Magn Reson Med 1992;23:37–45.
27. Bauer WR, Roder F, Hiller KH, Han H, Fröhlich S, Rommel E, Haase A, Ertl G. The effect of perfusion on T1 after slice-selective spin inversion in the isolated cardioplegic rat heart: measurement of a lower bound of intracapillary-extravascular water proton exchange rate. Magn Reson Med 1997;38:917–923.
28. Wacker CM, Wiesmann F, Bock M, et al. Determination of regional blood volume and intra-extracapillary water exchange in human myocardium using Feruglose: first clinical results in patients with coronary artery disease. Magn Reson Med 2002;47:1013–1016.
29. Francis ST, Bowtell R, Gowland PA. Modeling and optimization of Look-Locker spin labeling for measuring perfusion and transit time changes in activation studies taking into account arterial blood volume. Magn Reson Med 2008;59:316–325.
30. Healey JF. Statistics: a tool for social research. Belmont, CA: Wadsworth Publ.; 1999. xviii, p 540.
31. Chilian WM, Marcus ML. Phasic coronary blood flow velocity in intramural and epicardial coronary arteries. Circ Res 1982;50: 775–781.
32. Kampf T, Xavier, Ziener CH, Jakob PM, Bauer WR. Revisiting the determination of myocardial perfusion by T 1 based ASL methods applying Look-Locker readout. In Proceedings of the 20th Annual Meeting of ISMRM, Melbourne, Australia, 2012. Abstract 3499.